




Three-body bound states of quantum particles: Higher stability through braidingSophie Fisher , Olumakinde Ogunnaike *, and Leonid Levitov 
Massachusetts Institute of Technology, Cambridge, Massachusetts 02139, USA (Received 23 October 2023; revised 27 March 2024; accepted 1 April 2024; published 24 April 2024)

Motivated by recent cold atom experiments exploring the phase structure of Bose-Fermi mixtures, we propose novel emergent bound states. Cold atoms embedded in a degenerate Fermi system interact via a fermionic analog of the Casimir force, which is an attraction of a $-1/r$ form at distances shorter than the Fermi wavelength. Interestingly, the hydrogenic two-body bound states do not form in this regime because the interaction strength is too weak under realistic conditions, and yet the three-body bound states can have a considerably higher degree of stability. As a result, the trimer bound states can form even when the dimer states are unstable. A quasiclassical analysis of quantum states supported by periodic orbits singles out the figure-eight orbits, predicting bound states that are more stable than the ones originating from circular orbits. The discrete energies of these states form families of resonances with a distinct structure, enabling a direct observation of signatures of figure-eight braiding dynamics.

DOI: [10.1103/PhysRevA.109.043323](https://doi.org/10.1103/PhysRevA.109.043323)

Bose-Fermi mixtures have long been both practically important and theoretically a source of interesting and unconventional physics. Bose gases are often used to sympathetically cool down Fermi gasses to ultracold temperatures [1,2]. Theoretically, the fine control of ultracold atoms forming Bose-Fermi mixtures has made possible the exploration of a rich and varied phase diagram where bosons and fermions can bind to form fermionic molecules [3–6], polarons, and other novel bound states [7,8]. However, the phases dominated by bosonic physics and the bound states they host are not yet fully understood. Here, motivated by the recent experimental demonstration of a long-range attractive interaction between bosons [9] and observation of three-body resonances [10], we consider unusual bosonic bound states formed from this interaction in a weak coupling limit where $|a_{\text{eff}}| \ll R$, k_F^{-1} for effective boson scattering length, a_{eff} , and Fermi wave vector, k_F . One interesting aspect of this long-range interaction is that it behaves as a hydrogenic $-1/R$ potential at not too large distances.

The bound states within this regime are of considerable interest because of their simple, tunable hydrogenic character. Here we investigate the two-body and three-body states with the help of the semiclassical method. Interestingly, the limited range of distances in which the $1/R$ behavior holds proves to be more impactful for the dimer states than for the trimer states. Namely, one finds that two-body states may be rendered unstable, however, they can be stabilized by the addition of one more orbiting boson, leading to stable three-body bound states.

A remarkable prediction of quantum theory is that when the interactions between particles are not strong enough to support a two-body bound state, they may nonetheless support three-body bound states. This phenomenon has been explored in the framework of Efimov trimers [11,12]. Efimov trimers

are formed by particles interacting through short-range attractive interactions that are nearly resonant [11,12]. In this case, an infinite tower of three-body bound states forms even though two-body bound states are unstable. These trimer states have a peculiar nested shell structure related to discrete scale invariance and limit cycles in the renormalization group [13–15]. Efimov states have been a focus of active research in nuclear and cold atom physics, culminating in recent observations of a hierarchy of these states [16–18].

As we will see, the behavior in our problem is reminiscent of the physics behind Efimov trimers, where an unstable dimer is stabilized by an addition of a third particle. In our case, however, this stabilization is mediated by long-range interactions, whereas, for Efimov states, this stabilization is effected by short-range interactions. Interestingly, such short-range interactions also become relevant in our system, specifically in the alternate weak coupling limit where $R \ll |a_{\text{eff}}|$, k_F^{-1} [8].

The bound states discussed here have a very different character, originating from the long-range boson-boson interaction mediated by fermions. This interaction, being of an approximately $1/R$ character, supports two-body bound states resembling textbook hydrogenic states. In addition, one can envisage three-body states of various types stabilized by the near- $1/R$ attraction, as illustrated in Fig. 1. Among these, we consider three-body states that possess radial symmetry and the less conventional states, in which three particles move along a figure-eight trajectory in a fixed plane under the influence of $1/R$ attraction.

An important question pertaining to the detection of these dimer and trimer states is their stability. In a simplest framework, stability can be analyzed for the dimers and trimers completely isolated from other particles in the system. In this regime, the property of the boson-boson interaction that can potentially lead to instability is the weakening of the $1/R$ RKKY attraction at distances greater than the Fermi wavelength and, at the same time, the direct short-range boson-boson interaction. Interestingly, the impact of these

*Corresponding author: ogunnaik@mit.edu

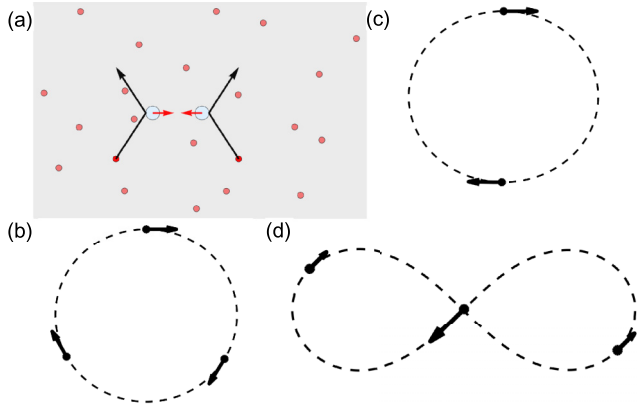


FIG. 1. (a) Schematic of attractive force between bosons (blue), mediated by the inward pressure due to scattering of fermions (red). (b) A two-body orbit. (c) A circular three-body orbit. (d) A figure-eight three-body orbit.

intrinsic effects on the stability of dimers is more pronounced than its impact on the stability of trimers. Namely, for a range of realistic interaction strengths, it can be shown that these two-body configurations are no longer stable bound states, while the three-body configurations remain proper bound states. Further, in realistic systems, dimers and trimers can also decay through nonintrinsic pathways due to scattering by surrounding atoms. Here, trying to keep discussion simple, we will only consider the intrinsic stability effects.

I. EFFECTIVE INTERACTION

Here we focus on bound states of two and three bosons embedded in a degenerate Fermi sea of cold atoms. Within the weak attraction limit with $|a_{\text{eff}}| \ll R, k_F^{-1}$, a fermion-mediated interaction arises through the so-called RKKY mechanism [19–21], giving

$$U(R) = -\frac{3\alpha}{(2k_F)^3} \frac{\sin(2k_FR) - 2k_FR \cos(2k_FR)}{R^4}, \quad (1)$$

where k_F is the Fermi momentum, and the interaction strength α depends on the boson-fermion scattering length and particle masses as discussed below. The fermion-mediated RKKY interaction between bosonic atoms was demonstrated in recent experiments with a Bose-Einstein condensate of Cs atoms embedded in a degenerate Fermi gas of Li atoms [9]. Further, triatomic Feshbach resonances have been observed in collisions between potassium (K) atoms and sodium potassium (NaK) diatomics, suggesting possible fermion-mediated bound states of two or more bosons [10]. As we will see, the bound states formed due to the RKKY interactions originate from classical orbit quantization and, therefore, form families of resonances with distinct structure.

In this case, in place of the short-range Efimov interaction, particles interact via a long-range interaction. Crucially, though this interaction is oscillatory at long distances, a simple Taylor expansion reveals that it is an attractive power law in R in a relatively wide range of distances, controlled by k_F . This can be seen by carrying out the expansion to lowest order

in $2k_FR \ll 1$:

$$U(R) = -\frac{\alpha}{R} \left(1 + \frac{(2k_FR)^2}{10} + \dots \right) \approx -\frac{\alpha}{R}. \quad (2)$$

This allows one to estimate the range of applicability of the $-1/R$ interaction as $2(k_FR)^2/5 \ll 1$. In other words, once bosons come approximately within one Fermi wavelength, k_F^{-1} , their attraction looks hydrogenic. Yet, if they come closer than the effective bosonic scattering length, a_{eff} , which includes the effect of the boson-fermion interaction, the original RKKY form is supplemented by a short-range attractive interaction leading to conventional Efimov states [8]. Typically in the weak interaction limit, this correction from the boson-fermion scattering is small ($|k_F a_{\text{BF}}| \ll 1$) and the effective scattering length closely approximates the bare boson-boson scattering: $|a_{\text{eff}}| \approx a_{\text{BB}}$. Thus, the $1/R$ attraction occurs within the range $|a_{\text{eff}}| \approx a_{\text{BB}} < R < k_F^{-1}$.

As a side remark, the origin of the $1/R$ attraction can be seen in a direct physical manner as a mutual shielding effect. Indeed, an anisotropy in the flux of fermions incident on the two bosonic atoms, with one atom shielding the other one, causes a net attractive force between the atoms via the fermionic Casimir effect [22,23]. This behavior is illustrated in Fig. 1(a).

II. BOUND STATES AND ORBITAL BRAIDING

Naturally, the behavior $U(R) \sim -1/R$ prompts the question of whether the two-particle bound states of a hydrogenic type, pictured schematically in Fig. 1(b), can occur. Nominally, the stability of such hydrogenic states would not depend on the interaction strength, α . However, since the radius of a hydrogenic states scales inversely with interaction strength, the α values do determine for which states $2k_FR > 1$. A simple expansion shows that the corrections to the hydrogenic potential from the full RKKY expression involve additional $(2k_FR)^2$ factors. These contributions can alter the behavior significantly if the Bohr radius, R_0 is too large. When $2k_FR \gg 1$, perturbation theory around hydrogenic states breaks down. Here, the RKKY interaction effectively falls off as $\cos(2k_FR)/R^3$, which decays too quickly and oscillates too rapidly between positive and negative values to support bound states. Our analysis indicates that α can be tuned by varying the fermion density and the boson-fermion scattering length to a point where the RKKY interactions are too weak to support two-body bound states. Surprisingly, however, the requirements for the formation of three-body bound states are not as stringent and such states can still persist under realistic conditions.

The stability of these three-body states stands in sharp contrast to that of the classical three-body problem. Classically, gravitational three-body orbits are made fragile by the lack of integrability of the three-body classical dynamics. Namely, three-body orbits are typically prone to decay into the more stable configurations of a two-body orbit and an unbound third body. However, in our problem this decay pathway is blocked in the absence of two-body bound states. As a result, strikingly, the quantum three-body orbits become more stable than the classical three-body orbits: our trimer states are effectively

stabilized by the absence of two-body bound states (a behavior similar to that of Efimov states).

Further, as we will see, the three-body states originating from the RKKY interaction are highly sensitive to orbit geometry. As appropriate for bound states supported by a long-range attraction, the underlying physics here can be best understood in a quasiclassical framework. Similar approaches have successfully been applied in the analysis of bound states [24–26]. Below, we apply quasiclassical quantization using the Gutzwiller trace formula framework. We consider, as primary examples, two simple periodic orbits of the three-body problem: the circular and the figure-eight orbits [27] pictured in Figs. 1(c) and 1(d), respectively. For both orbits the dynamics are locally stable, such that small perturbations remain small at all times.

These orbits share similar dynamic symmetry. The figure-eight orbit is a celebrated solution to the planar three-body problem in which three equal-mass particles travel around the same figure-eight curve with time shifts equal to $1/3$ of the period, as illustrated in Fig. 1(d).

The figure eight is the simplest periodic orbit in a large family discovered by Moore [27]. Originally it was located numerically using a functional gradient descent procedure described in Appendices; its existence was later confirmed by a rigorous analysis [28]. Circular orbits on which two and three particles are chasing each other with $1/2$ and $1/3$ period time shifts, as shown in Figs. 1(b), 1(c) provide a natural comparison to figure-eight orbits.

Our analysis of the quantum states associated with these orbits predicts Rydberg-like energy spectra

$$E_n = -C \frac{\alpha^2 m}{4\hbar^2 n^2}, \quad (3)$$

where the prefactor C depends on the orbit geometry and n is a positive integer with an upper bound where our approximation breaks down: $1 \leq n \leq n_{\max}$. For distinguishable particles n takes all positive integer values, whereas for identical bosonic particles $n = 1 + 3k$. The energy spectrum, Eq. (3), is written in a form that facilitates comparison with the conventional Rydberg spectrum. For two particles of equal masses, the latter is given by setting $C = 1$. For the three-body circular-orbit dynamics we find $C = 18$; for the figure-eight orbit we find $C \approx 34$. The large C values indicate that the three-body states are considerably more stable than the two-body states.

The difference in binding strengths can be traced to particles' orbit geometry and topology. Three particles moving along a circular orbit will clearly interact more strongly than two particles on the same orbit. Stronger binding for the figure-eight states as compared to the circular-orbit states can be attributed to the peculiar figure-eight braiding dynamics. The dynamics is such that the three particles come much closer to each other than particles moving along a circular orbit of comparable orbit size, which translates into a larger binding energy and higher stability.

These braiding dynamics should be contrasted with the schemes for braiding of particles with anyon statistics [29,30] or the physical braiding of qubits represented by trapped ions or the like to perform actions of quantum gates [31–34]. These operations typically require the intervention of an external source for confinement or control of the dynamics, while the

braiding described here may exist in an isolated system. The braiding described below illustrates the largely unexplored quantum-coherent phenomena for this RKKY interaction.

Further, we note that the simple hydrogenic $-1/R$ model for the fermion-mediated attraction, assumed in Eq. (3), is perfectly sufficient for assessing stability of low-lying states, a question that will be the focus of this paper. The RKKY interaction deviates from the simple model outside the range $2k_F R \ll 1$, where it falls off more rapidly than $1/R$. This behavior does not matter for the low-lying states so long as their localization radius is small enough: $2k_F R \ll 1$; yet, it is detrimental for the high- n states from Eq. (3) because a larger n translates into a larger orbit radius. For realistic α values, which are relatively small, we find that the spatial extent of all hydrogenic two-body states exceeds the Fermi wavelength, i.e., they fall outside the range $2k_F R \ll 1$ in which the $-1/R$ form holds. In contrast, for three-body states the value of α is high enough to push the orbit radius under the $2k_F R \ll 1$ bound for a finite number of low-lying states, ensuring their stability.

III. TWO-BODY STABILITY

To estimate the realistic interaction strength we use the parameter values from the recent experiment in which the fermion-mediated interaction was observed [9]. As shown in (2), within the appropriate radius, the interaction appears as a $-1/R$ potential with which we can analyze bound states for two and three bosonic particles

$$U(R) = -\frac{g_{\text{BF}}^2 m_F k_F^3}{3\hbar^2 \pi^3 R} = -\frac{\alpha}{R}, \quad \alpha = 0.0784 \frac{\hbar^2 a_{\text{BF}}^2 k_F^3}{m_p}, \quad (4)$$

where m_F and m_p are the masses of the fermion and proton, g_{BF} and a_{BF} are the boson-fermion coupling and scattering length, and k_F is the Fermi momentum.

It is instructive to start our discussion of the spectra by examining the two-body ground states. We estimate the typical boson separation by considering the Bohr's radius, R_0 with reduced mass, $\frac{m_B}{2}$:

$$\begin{aligned} 2k_F R_0 &= \frac{4\hbar^2 k_F}{m_B \alpha} = \frac{4 \times a_{\text{BF}}^{-2} k_F^{-2}}{133 \times 0.0784} \\ &= 1.39 \times 10^7 \left(\frac{a_0}{a_{\text{BF}}} \right)^2 \left(\frac{k_F^{(0)}}{k_F} \right)^2. \end{aligned} \quad (5)$$

Here, motivated by the form of α in Eq. (B9), we have chosen to normalize a_{BF} and k_F by Bohr's radius a_0 and $k_F^{(0)} \approx \pi \mu m^{-1}$, the value from Ref. [9].

Which parameter values can support states with radii in the range where our hydrogenic approximation holds? Choosing the realistic values $a_{\text{BF}} = 100a_0$ and $\frac{k_F}{k_F^{(0)}} = 10$ we find $2k_F R_0 \approx 14$. This value is too large to justify the approximation $2k_F R \ll 1$, indicating that no two-body bound states occur in this case. However, the conditions for confinement can be relaxed by tuning system parameters. Reference [9] suggests stable Bose-Fermi mixtures whose interaction agrees with perturbative calculations roughly in the range $-500a_0 < a_{\text{BF}} < 1000a_0$, outside of which, rapid losses cause heating of the BEC into a normal gas. Thus, choosing higher values

$a_{\text{BF}} = 500a_0$ and $k_{\text{F}} = 20k_{\text{F}}^{(0)}$, we obtain

$$2k_{\text{F}}R_0 = 0.14, \quad (6)$$

which is justifiably small. However, in this limit, our hydrogenic approximation is likely to be invalid for other reasons. If the orbit size is smaller than the effective bosonic scattering length, $R < |a_{\text{eff}}|$, the bosons come close enough to be sensitive to short-range forces that lead to qualitatively different bound states [8]. In addition, accessing such high values of a_{BF} and k_{F} may be practically challenging. Further discussion and spectral estimates for accessible three-body states may be found in Appendices.

IV. THREE-BODY STATES: SEMICLASSICAL QUANTIZATION

Next we discuss three-body bound states and argue that the conditions for supporting these states are less stringent than those for two-body states. The three-body states are described by the Hamiltonian

$$H(\mathbf{r}_i, \mathbf{p}_i) = \sum_i \frac{\mathbf{p}_i^2}{2m} + \sum_{i \neq i'} U(\mathbf{r}_i - \mathbf{r}_{i'}), \quad i, i' = 1, 2, 3. \quad (7)$$

We consider the long-range interactions $U(r) \sim -1/r$ and employ quasiclassical methods, wherein bound states arise from quantized periodic orbits. Importantly, unlike the two-body problem, the three-body problem is nonintegrable; as a result, the dynamics is chaotic in most of its phase space. Yet, islands of stability associated with certain periodic orbits are known to exist, giving rise to families of discrete states.

We analyze the three-body bound states using Gutzwiller's semiclassical quantization of nonintegrable Hamiltonian systems [35]. Gutzwiller's approach identifies the contribution to the density of states from quantum states associated with periodic orbits, which allows one to separate discrete states from the chaotic continuum. We apply this approach to the circular and figure-eight orbits pictured in Figs. 1(c) and 1(d). We first consider distinguishable particles; in this case the period of the orbit equals the time it takes each particle to undergo a full revolution. We then consider the case of indistinguishable particles. In this case, the period is reduced by 1/3, since the particles reach a permuted version of the initial point in phase space after a third of the period, and thus arrive at the same quantum state.

The Gutzwiller trace formula approximates the density of states of a nonintegrable Hamiltonian system as [35]

$$D(E) = \bar{D}(E) + \text{Re} \sum_p \frac{T_p}{\pi \hbar} \sum_{r=1}^{\infty} A_{p,r} e^{\frac{irS_p}{\hbar} - \frac{i\sigma_{pr}\pi}{2}}, \quad (8)$$

where p sums over all primitive (nonrepeated) periodic orbits with energy E , period T_p , action $S_p = \int \mathbf{p} \cdot d\mathbf{q}$, and r sums over all repetitions of a primitive orbit. Here σ_{pr} is the Maslov index for the r th repetition of the primitive orbit p , see Ref. [36]. The amplitude factor $A_{p,r} = |\det(M_p^r - 1)|^{-1/2}$ is a function of the stability matrix M_p that describes the local flow linearized about the primitive orbit p . The quantity $\bar{D}(E)$ is the average density of states of the system, which depends smoothly on energy (the Thomas-Fermi contribution

associated with the chaotic states). In our calculations, we will disregard this term because we only care about the oscillatory contribution to the density of states coming from the sum over classical periodic orbits. For simplicity, we set the amplitude factor $A_{p,r} = 1$ and also assume the Maslov index to be additive over successive repetitions r of a primitive orbit p ; denoting the index for one revolution of the orbit as $\mu \equiv \sigma_{p1}$ we write $\sigma_{pr} = r\mu$. The oscillatory contribution to the density of states is then given by a sum of terms multiplicative in r :

$$\delta D(E) = \text{Re} \sum_p \frac{T_p}{\pi \hbar} \sum_{r=1}^{\infty} \exp \left[ir \left(\frac{S_p}{\hbar} - \frac{\mu\pi}{2} \right) \right]. \quad (9)$$

This produces something akin to a saddle-point approximation, omitting slow amplitude variations to track phase variations on classical paths. The validity of the simplifying assumptions that lead to Eq. (9) will be discussed in detail elsewhere.

An essential property of periodic orbits allowing them to support discrete states is linear stability. While generally rare for periodic orbits of the three-body problem, this property holds for the orbits of interest. The stability of the three-body circular orbit is well known [27]; for the figure-eight orbits it was demonstrated in Refs. [37,38] by verifying that all eigenvalues of the stability matrix lie on the unit circle, and later proven rigorously in Ref. [39].

Another important aspect of our three-body problem is that orbits are unique up to symmetries of the equations of motion, including translation, rotation, and rescaling of the \mathbf{r}_i and \mathbf{p}_i variables

$$\mathbf{r}_i \rightarrow \frac{1}{\beta} \mathbf{r}_i, \quad \mathbf{p}_i \rightarrow \beta^{1/2} \mathbf{p}_i, \quad H \rightarrow \beta H. \quad (10)$$

We use this scaling symmetry to rewrite our trace formula in terms of a single reference orbit. Indeed, Eq. (10) defines a continuous family of orbits that are equivalent up to a rescaling. If $\mathbf{r}(t)$, $\mathbf{p}(t)$ define a solution with energy E , period T , and action S , then another solution is given by

$$\mathbf{r}'(t) = \beta^{-1} \mathbf{r}(\beta^{3/2}t), \quad \mathbf{p}'(t) = \beta^{1/2} \mathbf{p}(\beta^{3/2}t) \quad (11)$$

with energy $E' = \beta E$, period $T' = \beta^{-3/2}T$, and action $S' = \beta^{-1/2}S$, for any $\beta > 0$. This scaling has consequences for our trace formula. Because each orbit with energy E can contribute to the density of states only at $D(E)$, our calculations in Eq. (9) must incorporate the scaling relations. To proceed, we calculate the energy, period, and action of one particular reference orbit, which we label \bar{E} , \bar{T} , and \bar{S} . We define a scaling factor β for an orbit with energy E , taken relative to an orbit with energy \bar{E} , such that $\beta_E = E/\bar{E}$. Then the action and the period of the rescaled orbit can be written as

$$S_E = \beta_E^{-1/2} \bar{S}, \quad T_E = \beta_E^{-3/2} \bar{T}. \quad (12)$$

Focusing on the case of distinguishable particles, we can write the oscillatory contribution to the density of states from the entire family of figure-eight orbits:

$$\delta D(E) = \text{Re} \frac{\bar{T} \beta_E^{-3/2}}{\pi \hbar} \sum_{r=1}^{\infty} \exp \left[ir \left(\frac{\bar{S}}{\hbar} \beta_E^{-1/2} - \frac{\mu\pi}{2} \right) \right]. \quad (13)$$

The sum over repetitions r is a geometric series equal to

$$\delta D(E) = \text{Re} \frac{\bar{T} \beta_E^{-3/2}}{\pi \hbar} \frac{\exp \left[i \left(\frac{\bar{S}}{\hbar} \beta_E^{-1/2} - \frac{\mu \pi}{2} \right) \right]}{1 - \exp \left[i \left(\frac{\bar{S}}{\hbar} \beta_E^{-1/2} - \frac{\mu \pi}{2} \right) \right]}. \quad (14)$$

Poles of this expression describe the discrete energy spectrum of the bound states formed by particles confined to the orbit of interest.

V. THREE-BODY STATES: SPECTRAL ESTIMATES

From Eq. (14), we can calculate a spectrum using a reference orbit as input; however, the resulting spectrum should be independent of the reference orbit chosen. The poles of Eq. (14) lead to δ functions in the density of states whenever $\frac{\bar{S}}{\hbar} \left(\frac{\bar{E}}{E} \right)^{1/2} - \frac{\mu \pi}{2} = 2\pi n$. Rearranging this condition yields the energies E_n of an orbit with distinguishable particles, labeled by a quantum number n :

$$E_n = \frac{\bar{E} \bar{S}^2}{4 \hbar^2 \pi^2 \left(n + \frac{\mu}{4} \right)^2}. \quad (15)$$

Further focusing on the figure-eight solution and using the numerical method described in Appendices, we find $\bar{E} = -1.2935\alpha$ and $\bar{S} = 16.1609(\alpha m)^{1/2}$. The values \bar{E} and \bar{S} depend on the orbit used as an initial condition in the relaxation dynamics. However, their product $\bar{E} \bar{S}^2$ is a universal constant independent of the details of the procedure. Comparing to Eq. (3), we evaluate

$$C = \bar{E} \bar{S}^2 / \pi^2 \alpha^2 m = 34.23 \dots, \quad (16)$$

and set the Maslov index to its one-body and two-body value $\mu = 4$ (and shift $n + 1 \rightarrow n$) to yield our expected spectrum.

Our analysis of the figure-eight orbit can be easily extended to circular orbits. In the case of distinguishable particles, we need only calculate \bar{E} and \bar{S} for a reference radius, $r = 1$ in appropriate units, and plug these values into Eq. (15). We find values

$$\bar{E} = -\frac{3^{1/2} \alpha}{2}, \quad \bar{S} = 2\pi (3^{3/2} \alpha m)^{1/2}, \quad (17)$$

which gives $E_n = -9\alpha^2 m / 2 \hbar^2 (n + \frac{\mu}{4})^2$, which is nothing but Eq. (3) with $C = 18$.

We now consider how Eq. (15) must be modified for the case of indistinguishable particles. This is done by accounting for the permutation symmetry of the three-particle states. As noted above, the circular and figure-eight orbits share a dynamical symmetry. This shared symmetry allows us to consider either the circular orbit or figure-eight orbit with total period T and action S , where the particles start at the initial point (\mathbf{r}, \mathbf{p}) in phase space. After a time $T/3$, the particles reach a permuted version of the initial phase space point, $(P\mathbf{r}, P\mathbf{p})$, where P is the operator corresponding to the permutation (123). Since the particles are indistinguishable, the system has reached a quantum state identical to the initial state. Thus, we can think of $T/3$ as the new period of the system. Then the action of the system becomes $S/3$. Since the Maslov index for the modified orbit is one-third of the value for the original orbit, we replace \bar{S} with $\bar{S}/3$ and μ with $\mu/3$ in Eq. (15). This yields the spectrum in Eq. (3) with n taking values 1, 4, 7, 10, and so on.

A more intuitive way to arrive at this result is to consider the ground state for distinguishable particles for which the wave function is nodeless and is therefore identical to that for the ground state of bosonic particles. The number of nodes for the excited states, from permutation symmetry, must equal $3k$ for some positive integer k value, which leads to Eq. (3) with $n = 1 + 3k$ as above. These selection rules for quantum numbers reflect the permutation symmetry of the three-body states of identical bosons. One can view this property as a special case of the constraints on the three-body states due to braiding dynamics of identical particles.

Lastly, as a consistency check, we verify that these states lie within the regime of validity for our hydrogenic potential. Choosing the same values for the interspecies scattering length and the Fermi momentum as above, $a_{\text{BF}} = 100a_0$ and $\frac{k_{\text{F}}}{k_{\text{F}}^{(0)}} = 10$ and an effective scattering length within the uncertainty stated in [9], $|a_{\text{eff}}| \sim a_{\text{BB}} = 25a_0$, we check that they lie in the region of validity, approximately between the effective scattering length and Fermi wavelength: $25a_0 < R < 600a_0$. These estimates confirm that $\frac{(2k_{\text{F}}R_0)^2}{10} \ll 1$ and $\frac{R_0}{|a_{\text{eff}}|} \gg 1$. Starting from the relation in Eq. (5) and rescaling it by the factors of $C = 18$ and $C \approx 34$ for the three-body circular and figure eight of orbits gives

$$2k_{\text{F}}R_0 = \frac{1.39 \times 10^7}{C} \left(\frac{a_0}{a_{\text{BF}}} \right)^2 \left(\frac{k_{\text{F}}^{(0)}}{k_{\text{F}}} \right)^2. \quad (18)$$

Choosing the same values for the interspecies scattering length and the Fermi momentum as above, $a_{\text{BF}} = 100a_0$ and $\frac{k_{\text{F}}}{k_{\text{F}}^{(0)}} = 10$, we find $\frac{(2k_{\text{F}}R_0)^2}{10} \approx 0.06 \ll 1$ for the circular orbit and $\frac{(2k_{\text{F}}R_0)^2}{10} \approx 0.02 \ll 1$ for the figure-eight orbit. Scaling this relation by $2k_{\text{F}}a_{\text{eff}}$, with $|a_{\text{eff}}| \approx 25a_0$:

$$\frac{R_0}{|a_{\text{eff}}|} = \frac{4.16 \times 10^{10}}{C} \left(\frac{a_0}{a_{\text{eff}}} \right) \left(\frac{a_0}{a_{\text{BF}}} \right)^2 \left(\frac{k_{\text{F}}^{(0)}}{k_{\text{F}}} \right)^3. \quad (19)$$

With the values mentioned above, we find $\frac{R_0}{|a_{\text{eff}}|} \approx 9 > 1$ for the circular orbit and $\frac{R_0}{|a_{\text{eff}}|} \approx 5 > 1$ for figure-eight orbit. As such, the small values of $2k_{\text{F}}R_0$ and large values $\frac{R_0}{|a_{\text{eff}}|}$ of justify our $-1/R$ approximation. With the parameters mentioned above, the relevant energy scales for these bound states are as follows:

$$\tilde{\nu}_1 = C\nu_1 = 28.1 \text{ kHz} \quad (\text{circular three-body orbit})$$

$$\tilde{\nu}_1 = C\nu_1 = 53.5 \text{ kHz} \quad (\text{figure-eight orbit}). \quad (20)$$

However, as these were only estimates, potentially tighter confinement of the three-body states may enable higher binding energies and stability over two-body states.

VI. CONCLUSION AND DISCUSSION

We have shown that a mixed Bose-Fermi system tuned to the appropriate interspecies scattering length, a_{BF} , can give rise to bosonic bound states within a particular weak coupling limit where $|a_{\text{eff}}| \ll R, k_{\text{F}}^{-1}$. Further, one can tune the interaction such that none of these bound states is stable when only comprised of two particles, however, three-body states can be stable, and those with braiding semiclassical orbits even more so than standard circular orbits.

We attribute the higher stability of the figure-eight states, as compared to the ones on circular orbits, to the intertwining character of the braiding dynamics that brings particles much closer together for the same orbit radius. The three-body states are further stabilized by the lack of stable two-body states, as discussed above.

We emphasize the general character of our analysis, which can be applied to both other three-body orbits and the n -body problem. This is because the derivation of Eq. (15) depends only on the scaling properties of the system, and not on the number of particles.

Interestingly, the figure-eight orbit is known to exist in the n -body problem for all odd $n \geq 3$ [40], and one could thus use the same method to analyze the spectra of n -body bound states of the figure-eight orbit. As in the three-body case, quantum statistics of identical particles will manifest itself through holes in the discrete spectrum.

It should be noted that these states would still be subject to three-body losses that might hinder the observation of these states. Though we do not address these losses here, better understanding of the dynamical stability of these states would be an interesting and important step towards their experimental characterization.

Quantum states associated with these orbits, if realized in experiment, can provide a unique opportunity to demonstrate braiding that results directly from unitary quantum evolution and does not depend on external driving. The potential for braiding in three-body dynamics and the sensitivity to the different resulting geometries make these states particularly promising systems for further study.

ACKNOWLEDGMENTS

We are grateful to Alexander Turbiner, Chang Chin, and Vladan Vuletic for useful discussions. This work was supported by Science and Technology Center for Integrated Quantum Materials, National Science Foundation Grant No. DMR1231319.

APPENDIX A: ORBIT RELAXATION

The Gutzwiller trace formula relies on quantities such as the action, energy, and stability matrix eigenvalues of the periodic orbits of a dynamical system. To extract these quantities for a periodic orbit of the planar three-body problem, we require a numerical solution of the orbit, since in general no closed-form solution exists.

Here, we describe a numerical relaxation procedure for locating periodic orbits of the planar n -body problem in phase space, based off of work by Moore [27]. The procedure is a functional gradient descent that minimizes the action functional $S[\mathbf{r}_1(t) \dots \mathbf{r}_n(t)]$, where $\mathbf{r}_1(t) \dots \mathbf{r}_n(t)$ are the trajectories of n -point particles each with identical mass, m . We start by choosing fictional periodic orbits for each particle. To each orbit we apply a functional differential equation in fictional time τ :

$$\frac{d\mathbf{r}_i(t)}{d\tau} = \gamma \left(m \frac{d^2\mathbf{r}_i(t)}{dt^2} - \sum_{j \neq i} \mathbf{F}_{ij}(t) \right), \quad i, j = 1 \dots n, \quad (\text{A1})$$

where $\mathbf{F}_{ij}(t) = -\alpha \frac{\mathbf{r}_i(t) - \mathbf{r}_j(t)}{|\mathbf{r}_i(t) - \mathbf{r}_j(t)|^3}$ is the force from particle j acting on particle i at time t , and γ is a parameter that controls the descent rate. Once $d\mathbf{r}_i(t)/d\tau = 0$ for each $\mathbf{r}_i(t)$, the procedure has converged upon solutions to the equations of motion, since $m d^2\mathbf{r}_i(t)/dt^2 = \sum_{j \neq i} \mathbf{F}_{ij}(t)$. The right-hand side of Eq. (A1) can be rewritten as $-\frac{1}{m} \nabla S[\mathbf{r}_1(t) \dots \mathbf{r}_n(t)]$, where ∇S is the functional gradient or the variational derivative of S . The procedure is then a functional gradient descent, which decreases the action at each step until the procedure converges and the action reaches a local minimum.

As described by Moore, applying the procedure leads to a few possibilities, one of which is the convergence to a genuine periodic orbit of the system. In this case, the nature of the solution is determined by the topology of the initial orbit. In particular, if we plot the orbits of n bodies in the plane against time, the orbits draw out a braid of n strands in three-dimensional space time. This braid is a topological classification of the motion, which remains constant over the course of relaxation, as long as no collisions between particles occur. Other possibilities of applying relaxation are that two or more of the particles collide, causing a change in topology, or that one or more of the particles escapes to infinity. Escape occurs when the braid is separable, i.e., when the strands can be separated into two or more isolated subsets. For $1/r$ potentials, certain braids always lead to collision, forbidding any solution from having that braid type (the same is not true of strong-force $1/r^2$ potentials, where there is a solution for every braid). The reasons for this are discussed in detail by Moore and will not be the subject of this description.

In summary, the relaxation method is a relatively fast, accurate way of locating solutions to the planar n -body problem of a desired topology, allowing us to obtain the quantities necessary for the Gutzwiller trace formula. For instance, we can easily locate the three-body figure-eight solution by choosing initial trajectories of the form:

$$\mathbf{r}_1(t) = \begin{pmatrix} \sin(t - \frac{2\pi}{3}) \\ \sin(t - \frac{2\pi}{3}) \cos(t - \frac{2\pi}{3}) \end{pmatrix} \quad (\text{A2})$$

$$\mathbf{r}_2(t) = \begin{pmatrix} \sin(t) \\ \sin(t) \cos(t) \end{pmatrix} \quad (\text{A3})$$

$$\mathbf{r}_3(t) = \begin{pmatrix} \sin(t + \frac{2\pi}{3}) \\ \sin(t + \frac{2\pi}{3}) \cos(t + \frac{2\pi}{3}) \end{pmatrix} \quad (\text{A4})$$

for $0 \leq t \leq 2\pi$, where the trajectories are overlapping figure-eight orbits with period 2π , phase shifted from one another by $\frac{2\pi}{3}$. Applying the relaxation method converges to the true figure-eight solution with period 2π and energy $\bar{E} = -1.2935$ (for $\alpha = 1, m = 1$).

APPENDIX B: RKKY DERIVATION

The fermion-mediated RKKY interaction observed in Ref. [9] takes place between bosons in a Bose-Einstein condensate of cesium atoms and is mediated by the degenerate Fermi gas of lithium atoms in which they are embedded. The Hamiltonian for bosons embedded in a Fermi sea is of the form

$$H = H_B + H_F + H_{\text{int}}. \quad (\text{B1})$$

In a second-quantized form, the fermion and boson terms read

$$H_F = \int d^3r \phi^\dagger(\mathbf{r}) \frac{\mathbf{p}^2}{2m_F} \phi(\mathbf{r}),$$

$$H_B = \int d^3r \psi^\dagger(\mathbf{r}) \left(\frac{\mathbf{p}^2}{2m_B} + \frac{g_{BB}}{2} \psi^\dagger(\mathbf{r}) \psi(\mathbf{r}) \right) \psi(\mathbf{r}) \quad (\text{B2})$$

where $g_{BB} = \frac{4\pi\hbar^2 a_{BB}}{m_B}$ is the intraspecies coupling constant, a_{BB} is the corresponding scattering length, and $m_{B(F)}$ is the boson (fermion) mass. For our purposes, however, the interspecies interaction term is most important. To lowest order it reads:

$$H_{\text{int}} = g_{\text{BF}} \int d^3r \psi^\dagger(\mathbf{r}) \phi^\dagger(\mathbf{r}) \phi(\mathbf{r}) \psi(\mathbf{r}), \quad g_{\text{BF}} = \frac{2\pi\hbar^2 a_{\text{BF}}}{m_*} \quad (\text{B3})$$

with a_{BF} the interspecies scattering length, and $m_* = m_B m_F / (m_B + m_F)$ as the reduced mass. The fermion-mediated interaction can be obtained by integrating out the fermion degrees of freedom. To lowest order in the coupling g_{BF} , this gives an effective bosonic interaction [41]

$$\hat{H}_{\text{int}} \approx \frac{1}{2} \int d^3r d^3r' \psi^\dagger(\mathbf{r}) \psi^\dagger(\mathbf{r}') U(\mathbf{r} - \mathbf{r}') \psi(\mathbf{r}') \psi(\mathbf{r}), \quad (\text{B4})$$

where $U(R)$ is the RKKY interaction potential given by

$$U(R) = -3\alpha \frac{\sin(2k_F R) - 2k_F R \cos(2k_F R)}{R^4}, \quad (\text{B5})$$

with an explicit coupling strength given by

$$3\alpha = \frac{g_{\text{BF}}^2 m_F}{\hbar^2 (2\pi)^3}. \quad (\text{B6})$$

For the system studied in Ref. [9], the bosons are ^{133}Cs and the fermions are ^6Li . Taking $m_B = 113m_p$ and $m_F = 6m_p$, where m_p is the proton mass, gives the reduced mass $m_* \approx \frac{113 \cdot 6}{113+6} m_p \approx 5.7m_p$ and the coupling strength

$$g_{\text{BF}} = \frac{2\pi\hbar^2 a_{\text{BF}}}{5.7m_p}. \quad (\text{B7})$$

For small R , by carrying out the expansion to lowest order in $2k_F R \ll 1$,

$$\frac{\sin 2k_F R - 2k_F R \cos 2k_F R}{R^4} \approx \frac{(2k_F)^3}{3R}, \quad (\text{B8})$$

we can write $U(R)$ as a gravitational potential

$$U(R) = -\frac{g_{\text{BF}}^2 m_F k_F^3}{3\hbar^2 \pi^3 R} = -\frac{\alpha}{R}, \quad \alpha = 0.0784 \frac{\hbar^2 a_{\text{BF}}^2 k_F^3}{m_p}, \quad (\text{B9})$$

where we substituted the expression for the interspecies interaction strength g_{BF} , Eq. (B7).

From this interaction, we may derive the expected ground-state energy of a hydrogenic two-body state. Two interacting particles are described by the Hamiltonian

$$H = \frac{\mathbf{p}_1^2}{2m} + \frac{\mathbf{p}_2^2}{2m} + U(\mathbf{r}_1 - \mathbf{r}_2), \quad (\text{B10})$$

where from now on m labels the bosonic mass.

APPENDIX C: SPECTRAL ESTIMATES

The discrete energy spectrum is found readily by separating the center-of-mass motion, which, as mentioned in the main text, gives a hydrogenic Rydberg formula with a reduced mass for different orbit geometries, characterized by a constant, C ,

$$E_n = -\frac{C \alpha^2 m}{4 \hbar^2 n^2}, \quad n = 1, 2, 3, \dots \quad (\text{C1})$$

Where $C = 1$ for the two-body hydrogenic state. With this, we estimate the two-body ground-state frequency $\nu_1 = \frac{|E_1|}{2\pi\hbar}$ as

$$\nu_1 = \frac{\alpha^2 m}{4\hbar^3 (2\pi)} = \frac{133m_p}{8\pi\hbar^3} \left(\frac{0.0784 \cdot k_F^3 \hbar^2 a_{\text{BF}}^2}{m_p} \right)^2$$

$$\approx 1.56 \times 10^{-11} \left(\frac{a_{\text{BF}}}{a_0} \right)^4 \left(\frac{k_F}{k_F^{(0)}} \right)^6 [\text{Hz}], \quad (\text{C2})$$

where we have chosen to normalize the scattering length a_{BF} and the Fermi wave vector k_F by Bohr's radius a_0 and $k_F^{(0)} \approx \pi \mu\text{m}^{-1}$, the value from Ref. [9]. Choosing $a_{\text{BF}} = 100a_0$ and $k_F = 10k_F^{(0)}$, we find from Eq. (C2) the value $\nu_1 \approx 1.56 \text{ kHz}$, or in units of temperature, $h\nu_1/k_B \approx 1.16 \times 10^{-8} \text{ K}$. The frequencies for the circular three-body state and figure-eight state can easily be derived from this value as

$$\tilde{\nu}_1 = C\nu_1 = 28.1 \text{ kHz} \quad (\text{circular three-body orbit})$$

$$\tilde{\nu}_1 = C\nu_1 = 53.5 \text{ kHz} \quad (\text{figure-eight orbit}), \quad (\text{C3})$$

where the coefficients for the circular and figure-eight orbits are $C = 18$ and $C \approx 34.23$, respectively. If, instead, we choose higher values: $a_{\text{BF}} = 500a_0$ and $k_F = 20k_F^{(0)}$, we find a fairly large frequency value for the two-body state

$$\nu_1 = 6.24 \times 10^7 \text{ Hz}, \quad (\text{C4})$$

which in units of temperature is $h\nu_1/k_B = 4.6 \times 10^{-4} \text{ K}$. To find the radius for these conditions, we simply calculate the Bohr's radius for a reduced mass $\frac{m}{2}$.

$$R_0 = \frac{2\hbar^2}{m_B \alpha} = \frac{2 \cdot a_{\text{BF}}^{-2} k_F^{-3}}{133 \cdot 0.0784} = 2.2 \left(\frac{a_0}{a_{\text{BF}}} \right)^2 \left(\frac{k_F^{(0)}}{k_F} \right)^3 [\text{meters}], \quad (\text{C5})$$

where, we normalize the expression as in Eq. (C2). Then for the quantity $2k_F R$, which we previously approximated to be small, we have

$$2k_F R_0 = 2 \left(\frac{k_F}{k_F^{(0)}} \right) k_F^{(0)} R_0 = 1.39 \cdot 10^7 \left(\frac{a_0}{a_{\text{BF}}} \right)^2 \left(\frac{k_F^{(0)}}{k_F} \right)^2. \quad (\text{C6})$$

As noted in the main text, this yields $2k_F R_0 \approx 14$ for the former two-body conditions and $2k_F R_0 \approx 0.14$ for the latter. More generally, since the energy and orbital radius scale inversely, we should only expect stable, approximately hydrogenic orbits to exist in the regime where $a_{\text{BF}} \times k_F > \sqrt{\frac{10^7}{C}} (a_0 \times k_F^{(0)})$. Yet, this RKKY interaction is only expected to hold on length scales where $\frac{R}{a_{\text{eff}}} > 1$ [23]. When the average separation between bosons approaches the effective bosonic scattering length, many-body effects become more prominent

and a different potential function must be used [23]. The effective boson-boson scattering length is [9]

$$a_{\text{eff}} = a_{\text{BB}} - \frac{k_F (m_B + m_F)^2}{2\pi m_B m_F} a_{\text{BF}}^2$$

$$\stackrel{\frac{m_B}{m_F} \gg 1}{\approx} a_{\text{BB}} - \frac{m_B (k_F a_{\text{BF}})}{m_F} a_{\text{BF}}. \quad (\text{C7})$$

If we assume that a_{BB} and a_{BF} are of relatively similar size, then this implies that a_{eff} is determined by the bare boson-boson scattering length term, roughly when $\frac{m_B}{m_F} (k_F a_{\text{BF}}) \ll 1$, and determined by the boson-fermion scattering when $\frac{m_B}{m_F} (k_F a_{\text{BF}}) \gg 1$. If we choose a typical experimental value, $a_{\text{BB}} = 25a_0$ [9], then for $a_{\text{BF}} = 100a_0$ and $k_F = 10k_F^{(0)}$,

$$a_{\text{eff}} = a_{\text{BB}} - \frac{k_F (m_B + m_F)^2}{2\pi m_B m_F} a_{\text{BF}}^2 = -33a_0, \quad (\text{C8})$$

which is far smaller than the Bohr radius for any of the states described with these parameters. For $a_{\text{BF}} = 500a_0$ and $k_F =$

$20k_F^{(0)}$, we see

$$a_{\text{eff}} = a_{\text{BB}} - \frac{k_F (m_B + m_F)^2}{2\pi m_B m_F} a_{\text{BF}}^2 = -2907a_0, \quad (\text{C9})$$

whose magnitude is much larger than the two-body Bohr radius of $R_0 \approx 0.14/(2k_F) \approx 21a_0$. Thus, we expect the two-body state to be unstable in this regime.

More generally, we should be cautious of exiting the weak attraction limit: $k_F a_{\text{BF}} > 1$. To assure stable bound states exist we must attempt to self-consistently check that orbital radii, R , lie in the regime where $a_{\text{eff}} < R < k_F^{-1}$. This ensures that one remains in the appropriate limit required for the effective RKKY interaction. However, issues arise if one pushes to the regime where $(k_F a_{\text{BF}}) > 1$. Here, from Eq. (C7), without independently fine tuning a_{BB} , we expect bound states to exist roughly within a domain: $\frac{1}{2\pi} \frac{m_B}{m_F} (k_F a_{\text{BF}})^2 < k_F R < 1$. However, we have already assumed that $\frac{m_B}{m_F} \gg 1$ and $(k_F a_{\text{BF}}) > 1$, so this inequality cannot be satisfied.

-
- [1] F. Schreck, G. Ferrari, K. L. Corwin, J. Cubizolles, L. Khaykovich, M. O. Mewes, and C. Salomon, *Phys. Rev. A* **64**, 011402 (2001).
- [2] F. Schreck, L. Khaykovich, K. L. Corwin, G. Ferrari, T. Bourdel, J. Cubizolles, and C. Salomon, *Phys. Rev. Lett.* **87**, 080403 (2001).
- [3] K.-K. Ni, S. Ospelkaus, M. H. G. de Miranda, A. Pe'er, B. Neyenhuis, J. J. Zirbel, S. Kotochigova, P. S. Julienne, D. S. Jin, and J. Ye, *Science* **322**, 231 (2008).
- [4] J. W. Park, S. A. Will, and M. W. Zwierlein, *Phys. Rev. Lett.* **114**, 205302 (2015).
- [5] T. M. Rvachov, H. Son, A. T. Sommer, S. Ebadi, J. J. Park, M. W. Zwierlein, W. Ketterle, and A. O. Jamison, *Phys. Rev. Lett.* **119**, 143001 (2017).
- [6] K. F. Mak, K. He, C. Lee, G. H. Lee, J. Hone, T. F. Heinz, and J. Shan, *Nature Mater.* **12**, 207 (2013).
- [7] M. Duda, X. Chen, A. Schindewolf *et al.*, *Nature Phys.* **19**, 720 (2023).
- [8] T. Enss, B. Tran, M. Rautenberg, M. Gerken, E. Lippi, M. Drescher, B. Zhu, M. Weidemüller, and M. Salmhofer, *Phys. Rev. A* **102**, 063321 (2020).
- [9] B. J. DeSalvo, K. Patel, G. Cai, and C. Chin, *Nature (London)* **568**, 61 (2019).
- [10] H. Yang, D.-C. Zhang, L. Liu, Y.-X. Liu, J. Nan, B. Zhao, and J.-W. Pan, *Science* **363**, 261 (2019).
- [11] V. Efimov, *Phys. Lett. B* **33**, 563 (1970).
- [12] P. Naidon and S. Endo, *Rep. Prog. Phys.* **80**, 056001 (2017).
- [13] A. LeClair, J. María Román, and G. Sierra, *Phys. Rev. B* **69**, 020505(R) (2004).
- [14] P. F. Bedaque, H.-W. Hammer, and U. van Kolck, *Phys. Rev. Lett.* **82**, 463 (1999).
- [15] S. D. Glazek and K. G. Wilson, *Phys. Rev. Lett.* **89**, 230401 (2002).
- [16] B. Huang, L. A. Sidorenkov, R. Grimm, and J. M. Hutson, *Phys. Rev. Lett.* **112**, 190401 (2014).
- [17] S.-K. Tung, K. Jiménez-García, J. Johansen, C. V. Parker, and C. Chin, *Phys. Rev. Lett.* **113**, 240402 (2014).
- [18] R. Pires, J. Ulmanis, S. Häfner, M. Repp, A. Arias, E. D. Kuhnle, and M. Weidemüller, *Phys. Rev. Lett.* **112**, 250404 (2014).
- [19] M. A. Ruderman and C. Kittel, *Phys. Rev.* **96**, 99 (1954).
- [20] T. Kasuya, *Prog. Theor. Phys.* **16**, 45 (1956).
- [21] K. Yosida, *Phys. Rev.* **106**, 893 (1957).
- [22] D. Zhabinskaya, J. M. Kinder, and E. J. Mele, *Phys. Rev. A* **78**, 060103(R) (2008).
- [23] Y. Nishida, *Phys. Rev. A* **79**, 013629 (2009).
- [24] C. R. Reeg and D. L. Maslov, *Phys. Rev. B* **90**, 024502 (2014).
- [25] J. Cserti, B. Béni, A. Kormányos, P. Pollner, and Z. Kaufmann, *J. Phys.: Condens. Matter* **16**, 6737 (2004).
- [26] A. Kormányos, P. Rakyta, L. Oroszlány, and J. Cserti, *Phys. Rev. B* **78**, 045430 (2008).
- [27] C. Moore, *Phys. Rev. Lett.* **70**, 3675 (1993).
- [28] A. Chenciner and R. Montgomery, *Ann. Math.* **152**, 881 (2000).
- [29] B. Field and T. Simula, *Quantum Sci. Technol.* **3**, 045004 (2018).
- [30] J. Pachos, *Int. J. Quantum. Inform.* **4**, 947 (2006).
- [31] A. G. Fowler, M. Mariantoni, J. M. Martinis, and A. N. Cleland, *Phys. Rev. A* **86**, 032324 (2012).
- [32] A. Javadi-Abhari, P. Gokhale, A. Holmes, D. Franklin, K. R. Brown, M. Martonosi, and F. T. Chong, in *Proceedings of the 50th Annual IEEE/ACM International Symposium on Microarchitecture* (ACM, New York, 2017).
- [33] L.-M. Duan, *Phys. Rev. Lett.* **93**, 100502 (2004).
- [34] A. Lemmer, A. Bermudez, and M. Plenio, *New J. Phys.* **15**, 083001 (2013).
- [35] M. C. Gutzwiller, *J. Math. Phys.* **12**, 343 (1971).

- [36] S. C. Creagh, J. M. Robbins, and R. G. Littlejohn, *Phys. Rev. A* **42**, 1907 (1990).
- [37] T. Kapela and C. Simó, *Nonlinearity* **20**, 1241 (2007).
- [38] G. E. Roberts, *Ergodic Theor. Dyn. Sys.* **27**, 1947 (2007).
- [39] X. Hu and S. Sun, *Commun. Math. Phys.* **290**, 737 (2009).
- [40] C. Simó, in *European Congress of Mathematics*, edited by C. Casacuberta, R. M. Miró-Roig, J. Verdera, and S. Xambó-Descamps (Birkhäuser Basel, Basel, 2001), pp. 101–115.
- [41] S. De and I. B. Spielman, *Appl. Phys. B* **114**, 527 (2014).